

# Electrohydrodynamic model of vesicle deformation in alternating electric fields

Petia M. Vlahovska<sup>1</sup>  
Thayer School of Engineering  
Dartmouth College  
Hanover, NH 03755, USA

Rubèn Serral Gracià<sup>2</sup>, Said Aranda-Espinoza<sup>3</sup>, Rumiana Dimova  
Max Planck Institute of Colloids and Interfaces  
Science Park Golm  
14424 Potsdam, Germany

March 21, 2009

<sup>1</sup>Corresponding author. Address: Thayer School of Engineering, Dartmouth College, 8000 Cummings Hall Hanover, NH 03755, USA Tel.: (603) 646-9922 email: petia.vlahovska@dartmouth.edu

<sup>2</sup>Current address: Culgi B.V. P.O. Box 252 2300 AG Leiden, The Netherlands

<sup>3</sup>Current address: Adhesion Cellulaire, CNRS UMR 6212, INSERM U600, Université de la Méditerranée, Luminy, Marseille, France

## Abstract

We develop an analytical theory to explain the experimentally-observed morphological transitions of quasi-spherical giant vesicles induced by alternating electric fields (1). The model treats the inner and suspending media as lossy dielectrics, and the membrane as an impermeable flexible incompressible-fluid sheet. The vesicle shape is obtained by balancing electric, hydrodynamic, bending, and tension stresses exerted on the membrane. Our approach, which is based on force balance, also allows to describe the time evolution of the vesicle deformation, in contrast to earlier works based on energy minimization which are able to predict only stationary shapes.

Our theoretical predictions for vesicle deformation are consistent with experiment. If the inner fluid is more conducting than the suspending medium, the vesicle always adopts a prolate shape. In the opposite case, the vesicle undergoes a transition from a prolate to oblate ellipsoid at a critical frequency, which the theory identifies with the inverse membrane charging time. At frequencies higher than the inverse Maxwell-Wagner polarization time, the electrohydrodynamic stresses become too small to alter the vesicle's quasi-spherical rest shape. The model can be used to rationalize the transient and steady deformation of biological cells in electric fields.

*Key words:* lipid membrane; giant vesicle; electric field; electrodeformation; vesicle morphology

# 1 Introduction

Electric fields are widely used for cell manipulation. Weak fields influence cell signaling, wound healing, and cell growth (2–5). Strong pulsed fields can induce transient perforation of the cell membrane, which enables the delivery of exogenous molecules (drugs, proteins, and plasmids) into living cells (5, 6).

Biological cells exhibit various frequency-dependent behaviors in AC electric fields: orientation, translation (dielectrophoresis), and rotation. These phenomena have stimulated considerable modeling effort aimed at understanding of the physical mechanisms of the interaction of electric fields with cells and tissues. A common theme among different theoretical models is the assumption that the cell is a lossy dielectric particle of *fixed* shape (a sphere(7–10) or an ellipsoid(11, 12)). For example, the orientation of cells can be predicted by considering the torque on an ellipsoid due to the effective dipole moment induced by the electric field (13, 14); the dipole based theory has been successfully applied to interpret electro-orientation of erythrocytes (15).

Cells, however, are *soft* objects, which deform when subjected to electric fields. The cell membrane plays a critical role in this process. For example, the shear elasticity of the red blood cell membrane controls the cell electrodeformation (16–18). The lipid bilayer is the main structural component of the cell membrane, yet, the electrodeformation of closed pure lipid bilayer membranes (vesicles) has been considered only to a limited extent (19–21). There is increasing interest in this problem, particularly in relation to electropermeabilization (22–28). Recent experiments have shown that vesicle behavior in electric fields exhibits peculiar features. Vesicles subjected to a direct-current-electric pulse can deform into elliptical (29) or cylindrical shapes (30). Alternating-current-electric fields deform vesicles into prolate or oblate ellipsoids depending on the frequency and the conductivities of the interior and suspending fluids (1, 31, 32).

The physical mechanisms responsible for vesicle electrodeformations are not fully understood at present time. It is generally agreed that the prolate shape results from electrostatic pressure that pulls the vesicle at the poles, where the electric field is maximal. However, the oblate deformation, and in particular the fact that it is observed only when the enclosed fluid is less conducting than the suspending medium, has eluded adequate explanation. It has been proposed that anisotropy in the dielectric constant of the membrane is responsible for the oblate shapes (33), but this model can not explain the experimentally observed dependence on the conductivity ratio (1). Available theories do not account for the asymmetry in the fluids conductivities, and predict only prolate shapes (19–21). Moreover, these models employ an “energy” approach, according to which stationary shapes are computed by minimizing the sum of the membrane and electrostatic energies. Recently, unusual transient shapes of vesicles subjected to strong electric pulses have been observed (30). Explaining their existence goes beyond the scope of the equilibrium energy models. These transient features can be accounted for only by means of a truly non-equilibrium mechanical approach, which is based on force balance. To the authors knowledge, there is only one attempt to describe vesicle dynamics in electric fields (34). However, the model provides little physical insight because membrane deformation is described by a postulated ad hoc kinematic equation instead of the actual force balance.

In this paper we develop a theoretical explanation of the observed effects of AC electric fields on vesicle shapes. The transient vesicle deformation is determined by evaluating all forces (electric, hydrodynamic, bending, and tension) exerted on the membrane (35). Our model is motivated by the possibility for fluid flow driven by the electric field. Free charges, e.g., ions, tend to accumulate at interfaces separating media with different electric properties. The electric field acting on these free charges gives rise to fluid flow relative to the interface (36, 37). Electrohydrodynamic (EHD) flows have been observed long ago with drops (38, 39), and only recently reported for vesicles (40).

Drops adopt oblate shapes solely due to the EHD flow, as illustrated in Figure 1. We propose that the EHD flow is also responsible for the oblate vesicle shapes.

Notwithstanding the qualitative similarity between drops and vesicles, the extension of the EHD model from drops to vesicles is not a straightforward task because the mechanics of lipid membranes is far more complex than the mechanics of fluid-fluid interfaces. There are three major challenges. First, the lipid membrane is essentially an insulating shell impermeable to ions. When an electric field is applied, charges accumulate on both sides of the bilayer and the vesicle acts as a charging capacitor. Second, since the lipid bilayer contains a fixed number of molecules the vesicle area is constant and the membrane is area-incompressible. Under stress, the membrane develops nonuniform tension, which adapts itself to the forces exerted on the membrane in order to keep the local area constant. At steady state the gradients in tension counteract the flow-inducing tangential electric force and the electrohydrodynamic flow stops. Third, lipid membranes are extremely soft and can be easily bent by thermal noise. The area constraint implies an effective or entropic tension for fluctuations (41). Deformation of quasi-spherical vesicles in electric field results from flattening of the shape undulations, which increases the membrane tension (42). In strong electric fields, vesicle deformation is in fact limited by the large membrane tension. The theories based on the energy approach (21, 33) omit the tension and thereby exaggerate vesicle deformations (see (1), Supplementary material). Our approach rigorously accounts for these effects, and thus it is able to predict vesicle deformations consistent with experiment.

The paper is organized as follows: Section 2 describes the physical model and formulates the governing equations, Section 3 outlines the solution and discusses the frequency dependence of the electric stresses, and Section 4 shows the theory predictions and comparison with experiment for the vesicle shape as a function of frequency and conductivity ratio.

## 2 The model

### 2.1 The physical picture and characteristic time scales

Let us consider a giant vesicle with no net charge formed by a membrane with conductivity  $\lambda_{\text{mm}}$  and dielectric constant  $\epsilon_{\text{mm}}$ . The bilayer thickness is about  $h \sim 5\text{nm}$ , thus on the length scale of a cell-size vesicle (radius  $a \sim 10\mu\text{m}$ ) the bilayer membrane can be regarded as a two-dimensional surface with capacitance  $C_m = \epsilon_{\text{mm}}/h$  and conductivity  $G_m = \lambda_{\text{mm}}/h$ . The vesicle is filled with a fluid of viscosity  $\eta_{\text{in}}$ , conductivity  $\lambda_{\text{in}}$ , and dielectric constant  $\epsilon_{\text{in}}$ , and suspended in a different fluid characterized by  $\eta_{\text{ex}}$ ,  $\lambda_{\text{ex}}$ , and  $\epsilon_{\text{ex}}$ . The physical properties of the fluids and the membrane are assumed to be frequency-independent.

The vesicle is subjected to a uniform AC electric field with an amplitude  $E_0$

$$E^\infty = E_0 \cos(\omega t), \quad (1)$$

where  $\omega$  is the angular field frequency and  $t$  is the time. When an electric field  $E(t)$  is applied to an electrolyte solution, the free ions move parallel to the field. The ion redistribution leads to inhomogeneities in the bulk charge density, which decay on a time scale (36, 39)

$$t_{c,i} = \frac{\epsilon_i}{\lambda_i} \equiv \frac{l_{D,i}^2}{D}, \quad i = \text{in, ex} \quad (2)$$

where  $\epsilon$  and  $\lambda$  denote the absolute permittivity and conductivity of the fluid;  $l_D^2 = \epsilon k_B T / 2e^2 C$  is the Debye length (for a symmetric 1:1 electrolyte) and  $D$  is the electrolyte ions diffusivity (43). Here  $C$  is the salt concentration,  $e$  is the electronic charge,  $k_B$  is the Boltzmann constant, and  $T$  is

temperature. Hence, for frequencies  $\omega < 2\pi t_c^{-1}$ , the bulk solution is electroneutral and free charges are present only at boundaries that separate media with different electric properties. The rate of accumulation of charges at the interface of a macroscopic object, e.g., a sphere, is given by the Maxwell-Wagner polarization time (10)

$$t_{MW} = \frac{\epsilon_{in} + 2\epsilon_{ex}}{\lambda_{in} + 2\lambda_{ex}}. \quad (3)$$

The electric field acts on the free charges at the interface and gives rise to a force, which is tangential to the interface. In the case of a simple fluid-fluid interface, e.g., a drop, only a hydrodynamic force can balance the shearing electric force. As a result, the fluids are set in continuous motion, the so called electrohydrodynamic (EHD) flow (38). The EHD flow is characterized by a time scale, which corresponds to the inverse of the shear rate imposed by the tangential electric stress

$$t_{el} = \frac{\eta_{ex}}{\epsilon_{ex} E_0^2}. \quad (4)$$

In the case of drops and quasi-spherical vesicles, the flow inside is toroidal with a direction either from or towards the poles depending on the surface charge distribution as illustrated in Figure 1.

The membrane represents a more complex boundary compared to fluid-fluid interfaces. First, it is an insulating shell and charges accumulate on both the inner and outer surfaces, as illustrated in Figure 2. Hence, a vesicle of radius  $a$  acts as spherical capacitor that charges on a time scale given by (44, 45)

$$t_{cap} = aC_m \left( \frac{1}{\lambda_{in}} + \frac{1}{2\lambda_{ex}} \right). \quad (5)$$

Second, the membrane mechanics is governed by resistance to bending. A distortion of the membrane shape relaxes on a time scale

$$t_{\kappa} = \frac{\eta_{ex} a^3}{\kappa}, \quad (6)$$

where  $\kappa$  is the bending modulus. The curvature relaxation is controlled by the viscosity of the suspending fluid. In general, viscous dissipation takes place both in the embedding liquid and in the membrane (46). The relative importance of the bulk and membrane dissipation mechanisms is further discussed in Section 2.2.2.

It is instructive to estimate the magnitude of the characteristic time scales involved in vesicle electrodeformation. Typical experimental conditions involve fluids with conductivities in the range  $\lambda \sim 10^{-3} - 10^{-4} S/m$  and electric fields of the order of  $E \sim 1 kV/cm$  (1, 20, 30, 32, 47). In physiological conditions, e.g., blood, the internal conductivity of an erythrocyte is much higher  $\sim 0.5 S/m$  (15). The typical size of a vesicle or cell is  $a \sim 10 \mu m$ . The inner and outer fluids are essentially water: viscosity  $\eta \sim 10^{-3} Pa.s$ , and density  $\rho \sim 1000 kg/m^3$ . The membrane capacitance is  $C_m \sim 10^{-2} F/m^2$  (48) and bending rigidity  $\kappa \sim 10^{-19} J$ . Therefore, for vesicles, we estimate the basic charging time and the Maxwell-Wagner polarization time  $t_c \sim t_{MW} \sim 10^{-7} s$ , the membrane charging time  $t_{cap} \sim 10^{-3} s$ , the electrohydrodynamic time  $t_{el} \sim 10^{-3} s$ , and the bending relaxation time  $t_{\kappa} \sim 10 s$ .

We see that vesicle dynamics in electric fields involves processes that occur on very different times scales. Vesicle deformation takes place concurrently with fluid motion. The electric field adjusts to a new boundary configuration much faster than the fluid moves, because conduction (and hence charge redistribution) is fast,  $t_{MW} \ll t_{el}$ . Based on the time-scale separation, we can assume the electric field to be quasi-static and dependant only on the instantaneous vesicle shape. The flow time scale is comparable to the capacitor charging time,  $t_{el} \sim t_{cap}$ . The interplay between these two time scales is responsible for the observed dynamics of vesicles in electric fields (1).

## 2.2 Governing equations

In essence, our model consists of conservation of current, which obeys Ohm's law, and the Stokes equations to describe fluid motion (36). Charges carried by conduction accumulate at interfaces and bulk phases become electroneutral on a very fast time scale given by  $t_c$ , Eq. 2. Accordingly, the equations of bulk fluid motion have no electric terms and the electromechanical coupling occurs only at boundaries.

### 2.2.1 Electrohydrodynamic problem

**Electric field:** The electric potential,  $\Phi$ , for a quasi-static electromagnetic field is the solution of the Laplace equation

$$\nabla^2 \Phi = 0, \quad \mathbf{E} = -\nabla \Phi. \quad (7)$$

The membrane acts as a capacitor. Accordingly, the potential undergoes a jump across the interface

$$\Phi^{\text{in}} - \Phi^{\text{ex}} = \Delta \Phi(\omega, t) \quad \text{at} \quad r = r_s, \quad (8)$$

where  $r = r_s$  denotes the position of the interface in a coordinate system centered in the vesicle (see Fig. 2). The relation between the transmembrane potential and the membrane capacitance depends on geometry. The spherical shell is a widely used model for cells and vesicles (9, 44), although a spheroidal geometry has also been considered (11).

Free charges at the interface cause a discontinuity in the normal component of the displacement vector

$$\mathbf{n} \cdot [\epsilon_{\text{ex}} \mathbf{E}^{\text{ex}} - \epsilon_{\text{in}} \mathbf{E}^{\text{in}}] = Q(\omega, t) \quad \text{at} \quad r = r_s, \quad (9)$$

where  $\mathbf{n}$  is the outward unit normal vector and  $Q$  is the free charge density. Neglecting effects of charge convection along the surface by fluid motion, the conservation of electric currents at the interface requires that

$$\mathbf{n} \cdot [\lambda_{\text{ex}} \mathbf{E}^{\text{ex}} - \lambda_{\text{in}} \mathbf{E}^{\text{in}}] = -\frac{\partial Q}{\partial t} \quad \text{at} \quad r = r_s. \quad (10)$$

The forces due to an electric field  $\mathbf{E}$  are calculated from the Maxwell stress tensor

$$\mathbf{T}^{\text{el}} = \epsilon \left( \mathbf{E} \mathbf{E} - \frac{1}{2} \mathbf{E}^2 \mathbf{I} \right), \quad (11)$$

where  $\mathbf{I}$  denotes the unit tensor. A harmonic electric field can be written as

$$\mathbf{E} \cos(\omega t) = \frac{1}{2} (\mathbf{E} + \mathbf{E}^*), \quad (12)$$

where the superscript  $*$  denotes a complex conjugate. It gives rise to a non-zero time-averaged component of the Maxwell stress tensor

$$\mathbf{T}^{\text{el}}(\omega) = \frac{1}{4} [\mathbf{E} \mathbf{E}^* + \mathbf{E}^* \mathbf{E} - |E|^2 \mathbf{I}], \quad (13)$$

which is responsible for the steady deformation of the vesicle.

All electric variables (electric field, potential, charge density) vary harmonically with time  $u(\mathbf{r}, t, \omega) = \bar{u}(\mathbf{r}, \omega) \exp(i\omega t)$ . Hence, hereafter unless specifically stated, we will always refer to the amplitude of an electric variable,  $\bar{u}(\mathbf{r}, \omega)$ , and we will omit the bar for convenience.

**Hydrodynamic field:** Vesicle deformation is accompanied by motion in the surrounding fluids. The fluid velocity,  $\mathbf{v}$ , and pressure,  $p$ , inside and outside the vesicle are described by the Stokes equations (49, 50)

$$\rho \frac{\partial \mathbf{v}}{\partial t} = \nabla \cdot \mathbf{T}^{\text{hd}}, \quad \nabla \cdot \mathbf{v} = 0. \quad (14)$$

The bulk hydrodynamic stress is

$$\mathbf{T}^{\text{hd}} = -p\mathbf{I} + \eta[\nabla\mathbf{v} + (\nabla\mathbf{v})^\dagger], \quad (15)$$

where the superscript  $\dagger$  denotes transpose.

Eq. 14 is a simplified version of the more general Navier-Stokes equations. First, inertial effects are neglected because at the length-scale of the cell water is effectively very viscous. Second, the bulk stress has no contribution from the electric field because there are no excess free bulk charges. The unsteady term  $\partial\mathbf{v}/\partial t$  can be neglected provided that the viscous relaxation time,  $t_v = a^2\rho/\eta$ , is faster than the changes in the electric field, i.e.,  $\omega < t_v^{-1}$  (51). The linearity and quasi-steadiness of the Stokes equations, and the decoupling of the electric and hydrodynamic equations in the bulk greatly simplify the solution of the problem.

Far away from the vesicle, the fluid is at rest and the flow field vanishes,  $\mathbf{v}^{\text{ex}} \rightarrow 0$ . In the absence of bilayer slip and membrane permeability, the velocity is continuous across the interface

$$\mathbf{v}^{\text{in}} = \mathbf{v}^{\text{ex}} \equiv \mathbf{v}_s \quad \text{at} \quad r = r_s. \quad (16)$$

The interface moves with the normal component of the velocity of the adjacent fluid (52)

$$\frac{\partial r_s}{\partial t} = \mathbf{v}_s \cdot \mathbf{n}. \quad (17)$$

Membrane permeability can be neglected in the case of osmotically stabilized vesicles and pore-free membranes, i.e., membranes in which the electric-field induced tension does not exceed the poration threshold.

**Electromechanical coupling:** The vesicle shape is determined by the balance between electric, hydrodynamic, and membrane tractions (surface force densities) at the interface  $r = r_s$

$$\mathbf{n} \cdot [(\eta_{\text{ex}}\mathbf{T}^{\text{hd,ex}} - \eta_{\text{in}}\mathbf{T}^{\text{hd,in}}) + (\epsilon_{\text{ex}}\mathbf{T}^{\text{el,ex}} - \epsilon_{\text{in}}\mathbf{T}^{\text{el,in}})] = \boldsymbol{\tau}^{\text{mem}}, \quad (18)$$

where flexoelectric bending of the lipid bilayer is neglected (53, 54). For example, at rest, when the electric field is off, Eq. 18 reduces to the familiar Euler–Lagrange equation (46), which states that there can be a jump in the hydrostatic pressure across a membrane due to membrane tractions

$$p^{\text{in}} - p^{\text{ex}} = 2\sigma H - \kappa [4H^3 - 4KH + 2\nabla_s^2 H]. \quad (19)$$

where  $\kappa$  is the bending rigidity,  $H$  and  $K$  are the mean and Gaussian curvatures. In the next section we discuss the membrane stresses in more detail.

### 2.2.2 Membrane mechanics

The pure lipid membrane consists of two sheets of lipid molecules. It stores elastic energy in bending, and dissipates energy by membrane surface viscosity and intermonolayer friction.

Within the framework of the minimal model (55), the bending resistance gives rise to a surface force density

$$\boldsymbol{\tau}^\kappa = -\kappa (4H^3 - 4KH + 2\nabla_s^2 H) \mathbf{n}. \quad (20)$$

The surface gradient operator is defined as  $\nabla_s = \mathbf{I}_s \cdot \nabla$ , where the matrix  $\mathbf{I}_s = \mathbf{I} - \mathbf{nn}$  represents a surface projection.

The membrane leaflets consist of fixed number of lipids, which are optimally packed with fixed area per lipid (under moderate stresses). As a result, a membrane element only deforms but can not change its area. Under stress, the membrane develops tension, which adapts itself to the forces exerted on the membrane in order to keep the local and total area constant. Hence, the tension is non-uniform along the interface and varies with forcing. The membrane tension gives rise to surface force density

$$\boldsymbol{\tau}^\sigma = 2\sigma H\mathbf{n} - \nabla_s \sigma. \quad (21)$$

where  $\sigma$  denotes the local membrane tension

For lipid bilayers in the fluid phase, the lipids are free to move within the monolayer. Therefore, in contrast to gel-phase lipid membranes, a fluid bilayer membrane has no shear-elastic modulus (31). Moreover, the surface viscosity of lipid bilayers in the fluid phase is relatively low,  $\eta_{mm} \sim 10^{-9} Ns/m$ , and its effects are usually negligible.

In addition to surface viscosity, other dissipation mechanisms are drag between the two monolayers (56) and permeation through the membrane. Dissipation by intermonolayer friction becomes important if bilayer shape changes occur on a time scale comparable to the lateral lipid redistribution within the bilayer (56–58). Vesicle deformation occurs on the electrohydrodynamic time scale,  $t_{el} \sim 10^{-3}s$  (for the experiments of Aranda et al. (1)). The bilayer slip time scale is  $t_{slip} = ba^2/K_A \sim 0.1s$ , where  $K_A \sim 0.1N/m$  is the bilayer stretch modulus and  $b \sim 10^8 N.s/m^3$  is the bilayer slip coefficient (31, 59). Based on large separation of time scales,  $t_{slip} \gg t_{el}$ , the bilayer slip was not included in the current model.

Membranes become permeable when subjected to sub-millisecond strong DC pulses that cause poration (29, 48, 60, 61); electropermeabilization in AC fields is less likely (62, 63). Pores form when the transmembrane potential exceeds a critical value, which for a tension-free membrane is  $V_c \sim 1V$  and decreases with initial tension (29, 48). Thus, in principle, it is possible to reach  $V_c$  in low-frequency AC field, where  $V_c \sim 3/2E_0a$ , provided that the electric field strength is higher than  $10^5 V/m$ . In the experiments of Aranda et al. (1), the electric field strengths were lower,  $2 \times 10^4 V/m$ , and vesicles were fluctuating which implies very low initial tensions. Hence, in this case membrane permeation appears unlikely and we have neglected it in this study. In addition, the vesicle volume as observed in experiments remained constant indicating no leakage through the membrane.

In summary, the external electric energy is stored in the membrane due to developing tension and bending moments, and dissipated by viscous friction in the bulk fluid. The bulk hydrodynamic dissipation prevails because the viscous relaxation time of the embedding fluids,  $t_v = a^2\rho/\eta \sim 1\mu s$ , is much shorter than the time scales associated with dissipation in the membrane.

### 2.3 Dimensionless parameters

It is more convenient to describe the problem in terms of non-dimensional parameters. Casting equations in dimensionless form helps show the generality of application to a broad class of situations rather than just one set of dimensional parameters.

Henceforth, bending stresses and tension are normalized by  $\kappa/a^2$ ; all other quantities are rescaled using  $\eta_{ex}$ ,  $\epsilon_{ex}$ ,  $\lambda_{ex}$ ,  $a$ , and  $E_0$ . The fluid velocity scale is  $v_0 = \epsilon_{ex}E_0^2a/\eta_{ex}$ . The electric and viscous stresses are rescaled by  $\epsilon_{ex}E_0^2$ . Time and frequency are nondimensionalized with the basic charging time  $t_c = \epsilon_{ex}/\lambda_{ex}$ .

The electric capillary number compares the shape-preserving bending stresses to the shape-distorting electric stresses,

$$Ca = \frac{t_\kappa}{t_{el}} = \frac{\epsilon_{ex} E_0^2 a^3}{\kappa}. \quad (22)$$

The other relevant parameters are the ratios of the electric properties of inner and outer fluid

$$\Lambda = \frac{\lambda_{in}}{\lambda_{ex}}, \quad S = \frac{\epsilon_{in}}{\epsilon_{ex}} \quad (23)$$

and the viscosity ratio

$$\chi = \frac{\eta_{in}}{\eta_{ex}}. \quad (24)$$

The dimensionless membrane conductivity and capacitance per unit area are

$$G_m = \frac{\lambda_{mm}}{x\lambda_{ex}}, \quad C_m = \frac{\epsilon_{mm}}{x\epsilon_{ex}}, \quad (25)$$

where the dimensionless membrane thickness is  $x = h/a$ .

We estimate that  $Ca \sim 10^3 \gg 1$  from the typical values discussed at the end of Section 2.1 that correspond to the experiments of Aranda et al. (1); the dielectric constants and viscosity ratios are  $S, \chi \sim 1$ , but the conductivity ratio vary between  $10^{-3}$  and 100.

### 3 Solution for small deformations

In a coordinate system centered at the vesicle, the radial position  $r_s$  of the vesicle interface is described by

$$r_s = 1 + f(\theta, \phi), \quad (26)$$

where  $f$  is the deviation of vesicle shape from a sphere. For a nearly spherical vesicle,  $f \ll 1$ . In this case, the exact position of the interface is replaced by the surface of a sphere of equivalent volume, and all quantities that are to be evaluated at the interface of the deformed vesicle are approximated using a Taylor series expansion. The solution for electric and flow fields is derived as a regular perturbation expansion in some small parameter, e.g., the excess area.

In this study we perform the leading order analysis. Accordingly, the electric and hydrodynamic fields are evaluated about a sphere. First, we determine the electric field and the electric tractions (surface force density) exerted on the membrane. Second, we determine the hydrodynamic tractions needed to satisfy the force balance Eq. 18 and the corresponding velocity field. Finally, we use the kinematic condition Eq. 17 to find the shape evolution.

In Eq. 26, the function  $f$  representing the perturbation of the vesicle shape depends only on angular coordinates. Thus, it is expanded into series of scalar spherical harmonics  $Y_{jm}$  given by Eq. 46 in Appendix B

$$f = \sum_{j=2}^{\infty} \sum_{m=-j}^j f_{jm} Y_{jm}, \quad (27)$$

Solutions for the electric field are growing and decaying harmonics which derive from  $\nabla(r^j Y_{jm})$  and  $\nabla(r^{-j-1} Y_{jm})$ . The uniform applied electric field along the  $z$ -direction, defined by Eq. 1, is described by the  $j = 1$  harmonic

$$\mathbf{E}^\infty = d^\infty \nabla(r Y_{10}), \quad d^\infty = \sqrt{\frac{4\pi}{3}} \quad (28)$$

Accordingly, the induced electric field has  $j = 1, m = 0$  symmetry.

### 3.1 Electrostatic field and stresses

The model for the electric field is based on the classic works by Schwan and coworkers (44). They have shown that an external AC electric field induces a potential across the membrane of a spherical shell (64),

$$\Delta\Phi = V_m(\omega) \cos\theta, \quad (29)$$

where

$$V_m(\omega) = \frac{3}{2} \frac{1}{1 + (G_m + i\omega C_m)(1/\Lambda + 1/2)}. \quad (30)$$

The transmembrane potential is very sensitive to the membrane thickness. Figure 3.a illustrates the variation of the transmembrane potential with frequency for a vesicle with a fixed size and two values of the membrane thickness, corresponding to a giant unilamellar lipid vesicle and a polymersome. For a simple fluid-fluid interface (a drop, i.e.,  $x = 0$ ), the transmembrane potential is zero.

The electric tractions exerted on the membrane have radial and tangential components

$$\boldsymbol{\tau}^{\text{el}} = \tau_r^{\text{el}} [1 + 3 \cos(2\theta)] \hat{\mathbf{r}} + \tau_\theta^{\text{el}} \sin(2\theta) \hat{\boldsymbol{\theta}}. \quad (31)$$

In terms of the electric field, the electric pressure can be written as

$$\tau_r^{\text{el}} = \frac{1}{2} [(E_r^{\text{ex}})^2 - (E_\theta^{\text{ex}})^2 - S((E_r^{\text{in}})^2 - (E_\theta^{\text{in}})^2)], \quad (32)$$

and the tangential electric force is

$$\tau_\theta^{\text{el}} = E_\theta^{\text{ex}} Q + S E_r^{\text{in}} V_m(\omega) \sin\theta, \quad (33)$$

where we have used the definition of surface charge  $Q$  given by Eq. 9. The amplitudes of the electric tractions,  $\tau_r^{\text{el}}$  and  $\tau_\theta^{\text{el}}$ , depend only on the electric properties of the media. Their expressions are given by Eq. 51 and Eq. 52 in Appendix C.1.

The electric stresses are complicated functions of the frequency  $\omega$  as illustrated in Figures 4.a and 4.b. We can distinguish three regimes:

*Low frequencies,  $\omega < \omega_1$ :* In this case, the membrane shields the vesicle interior and the electric field inside zero, as seen from Figure 3.b. The electric pressure is positive at the poles, and negative at the equator, thus pulling the vesicle into a prolate shape. The tangential electric stress is zero everywhere on the surface, because both induced charge and internal electric field are zero. In contrast, the tangential electric stress at a simple fluid-fluid interface, i.e., zero-membrane-thickness, is non-zero even at low frequencies, see Eq. 54. For conductivity ratio  $\Lambda < 1$ , the electric pressure changes sign and the tangential electric traction becomes significant above a frequency  $\omega_1$  given by (9, 44)

$$\omega_1 = \frac{G_m}{C_m} + \frac{2\Lambda}{C_m(\Lambda + 2)}, \quad (34)$$

which reduces to  $1/t_{\text{cap}}$ , Eq. 5, if the membrane is non-conducting.

*Intermediate frequencies,  $\omega_1 < \omega < \omega_2$ :* In this frequency window, the membrane capacitor becomes “short-circuited” and the vesicle interior participates in the conduction process. The onset of decrease in the transmembrane potential and increase in the interior electric field coincides with the appearance of tangential electric tractions, as seen in Figures 3 and 4. The tangential electric stress is mainly due to the free charges on the membrane (38), see Eq. 33. Because of the different conductivities of the inner and outer fluids, charges accumulate at different rates on

the membrane physical surfaces. As a result, charge densities on the inner and outer membrane surfaces can become imbalanced, which gives rise to a non-zero effective interfacial charge density as shown in Figure 5. The effective charge is zero at low frequencies because the membrane capacitor is fully charged, having equal charge densities on the inner and outer membrane surface, and at high frequencies because of insufficient time for interface charging.

*High frequencies,  $\omega > \omega_2$ .* The inverse Maxwell-Wagner polarization time, Eq. 3, defines a critical frequency

$$\omega_2 = \frac{\Lambda + 2}{S + 2}, \quad (35)$$

above which tangential stress starts to decrease. It vanishes at very high frequencies, where all media behave as perfect dielectrics. In this frequency regime, the electric pressure is small, but positive with magnitude  $\sim (S - 1)^2 / (S + 2)^2$ , which leads to small prolate deformation.

### 3.2 Hydrodynamic field and vesicle deformation

The stress balance at the interface Eq. 18 shows that the electric tractions need to be compensated by membrane and hydrodynamic forces. The latter can be found using the general solution for a nearly spherical vesicle subject to an external field (46, 65–67). Details of the solution are presented in the Supplementary material.

The vesicle area,  $A$ , exceeds the area needed to enclose the volume of the interior fluid,  $4\pi a^2$ . At rest, the excess area is redistributed among all shape modes

$$\Delta = A/a^2 - 4\pi = \sum_{j=2}^{\infty} \sum_{m=-j}^j \frac{(-1)^m}{2} (j-1)(j+2) f_{jm} f_{j-m}. \quad (36)$$

Therefore, in order to accurately describe vesicle deformation, in general, we need the evolution equations for all shape modes. These are derived in (65) (see also the Supplementary material) and have the general form

$$\frac{\partial f_{jm}}{\partial t} = C_{jm} + Ca^{-1}(\Gamma_1 + \sigma_h \Gamma_2) f_{jm} + O(f^2). \quad (37)$$

The first term describes the distortion of the vesicle shape by the electrohydrodynamic flow. The term including  $Ca$  is associated with shape relaxation driven by the membrane stresses. The coefficients  $C_{jm}$ ,  $\Gamma_1$ , and  $\Gamma_2$  are listed in the Supplementary material. The effective tension  $\sigma_h$  depends on the vesicle shape, which in turns depends on the applied electric field.

In general, the apparent area of a vesicle,  $\bar{A}$ , is lower than its true area,  $A$ , because of suboptical fluctuations in the shape modes. For example, a quasi-spherical vesicle at equilibrium is characterized by a zero apparent area, i.e.,  $\bar{\Delta} = 0$ . However, even though the membrane is inextensible, the vesicle can deform and increase its apparent area due to flattening of the shape undulations. This leads to an increase in the membrane tension (42)

$$\sigma_h = \sigma_0 \exp \left[ \frac{8\pi\kappa}{k_B T} \left( \frac{\bar{A}(t)}{4\pi a^2} - 1 \right) \right] = \sigma_0 \exp \left( \frac{2\kappa \bar{\Delta}}{k_B T} \right), \quad (38)$$

where  $\sigma_0$  is the initial tension in the membrane.

In the next section we simplify the theory for the case of vesicle electrodeformation induced by an uniform AC electric field.

## 4 Results

### 4.1 Deformation of a quasi-spherical vesicle

When the electric field is turned on, it generates electrohydrodynamic flow with the same symmetry as the electric stresses. The corresponding fluid velocity, which is responsible for the vesicle deformation, is given by

$$C^{\text{el}} \equiv C_{20} = 8\sqrt{\frac{\pi}{5} \frac{6\tau_r^{\text{el}} - \tau_\theta^{\text{el}}}{23\chi + 32}}, \quad (39)$$

where the electric stresses are given by Eq. 51 and Eq. 52 in Appendix C.1, and the viscosity parameter  $\chi$  is defined by Eq. 24. Since electric stresses directly affect only the ellipsoidal  $j = 2$ ,  $m = 0$  mode, the most important contribution to the vesicle deformation comes from the ‘‘elongational’’  $f_{20}$  mode. Moreover, because the shape modes are coupled through the area constraint Eq. 36, the area stored in the  $j \neq 2$  modes is transferred into the ellipsoidal  $f_{20}$  mode. The maximum possible vesicle deformation corresponds to elongation where all excess area is stored in the  $f_{20}$  mode

$$f_{20}^{\text{max}} = \pm\sqrt{\frac{\Delta}{2}}, \quad (40)$$

where a positive sign corresponds to a prolate deformation.

The shape evolution strongly depends on the effective tension  $\sigma_h$ . For a quasi-spherical vesicle, using the relation between excess area and shape modes Eq. 36, and including only the dominant contribution from the  $f_{20}$  mode, we can rewrite Eq. 38 as

$$\sigma_h = \sigma_0 \exp\left(\frac{4\kappa}{k_B T} f_{20}^2\right). \quad (41)$$

Inserting into Eq. 37 we obtain that the shape evolution of a vesicle in AC electric field is described by the following non-linear equation

$$\frac{\partial f_{20}}{\partial t} = C^{\text{el}} - Ca^{-1} \frac{24 \left[6 + \exp\left(\frac{4\kappa}{k_B T} f_{20}^2(t)\right)\right]}{23\chi + 32} f_{20}(t). \quad (42)$$

At steady state  $\partial f_{20}/\partial t = 0$ , and the stationary vesicle shape is given by

$$f_{20} = \sqrt{\frac{\pi}{5} \frac{6\tau_r^{\text{el}} - \tau_\theta^{\text{el}}}{3(6 + \sigma_h)}}. \quad (43)$$

The above equation is a generalization of the relation derived by Kummrow and Helfrich(20), which is valid only for frequencies lower than  $\omega_1$ .

### 4.2 Discussion

The shape evolution obtained from Eq. 42 for several frequencies is illustrated in Figure 6.a. We observe that a vesicle deforms on a hydrodynamic time scale approximated by  $t_d = 1/C^{\text{el}}$ . The final steady deformation depends on the strength of the deforming electric stresses, which decrease with frequency. The time needed to reach stationary shape depends strongly on the viscosity contrast between the inner and outer fluid. Figure 6.b shows that increasing the viscosity of the inner fluid slows down the shape evolution. The viscosity effect may become important in the electrodeformation of red blood cells, which are characterized by  $\chi \sim 10$ .

The steady shape of a vesicle in AC electric field is calculated by evaluating Eq. 42. Figure 7 illustrates the steady shapes of vesicles in AC field as a function of frequency for different conductivity ratios. The theory predicts that the type of deformation, prolate or oblate, is determined primarily by the frequency and the conductivity ratio. At low frequencies  $\omega < \omega_1$  the deformation is prolate. For frequencies  $\omega > \omega_1$  vesicles are prolate or oblate depending on the conductivity ratio. At even higher frequencies, the deformation becomes again prolate but very small and the vesicle appears spherical.

Next we analyze these morphological transitions in more detail.

#### 4.2.1 Prolate-oblate transition for $\Lambda < 1$ at low frequencies

The transition frequency  $\omega_1$  corresponds to the capacitor charging time Eq. 34.

At low frequencies,  $\omega < \omega_1$ , vesicle deformation is due solely to the positive electric pressure. It is maximal at the poles, see Eq. 51 in Appendix C.1. The vesicle is pulled apart and thus adopts a prolate ellipsoidal shape.

At  $\omega > \omega_1$ , the tangential electric traction becomes significant and the electric pressure is negative, as seen from Figure 4. The shearing tangential force induces electrohydrodynamic flow, similar to the one observed with drops (Figure 1). If  $\Lambda/S < 1$  the flow is directed from the poles to the equator and the resulting deformation is oblate; if  $\Lambda/S > 1$  the flow is directed from the equator to the poles and the resulting deformation is prolate. Therefore, prolate-oblate transition is possible only if  $\Lambda/S < 1$ . In experiments with vesicles(1, 30, 32), the inner and outer fluids are sucrose and glucose, which have similar dielectric constant,  $S \sim 1$ . Oblate shapes were reported for conductivity ratio less than 1, in agreement with the condition  $\Lambda/S < 1$ . In the case of biological cells, the difference between the dielectric constants of the cytosol and the cell environment is also small, and therefore similar deformation behavior is expected. In the case of drops, the electrohydrodynamic flow persists for as long as the electric field is applied because only viscous stresses can balance the tangential electric surface force. In contrast to drops, the electrohydrodynamic flow in vesicles is not sustained. It stops when the vesicle reaches steady deformation because the membrane tension counteracts the electric tangential force.

The capacitor charging time decreases with the size of the vesicle. Therefore, the smaller the vesicle, the higher the transition frequency. For nanometer size vesicle this frequency is in the MHz range. Thus, nano-vesicles are expected to deform only into prolate ellipsoids when subjected to AC fields with frequency less than a MHz or DC pulses with length longer than  $1 \mu s$ , which is in agreement with experimental observations (68).

#### 4.2.2 Comparison with experiment

Figures 8 and 9 demonstrate that our theory is consistent with the experiment. Our model captures the morphological transitions of vesicles in AC fields, in particular, the prolate-oblate one at low frequencies. The theory also shows that vesicles should be spherical at high-frequencies as experimentally observed. In addition, it correctly predicts the effect of conductivity on the type of deformation, which has not been reported by other models.

Figure 8 shows the dependence of the vesicle deformation on field frequency and conductivity ratio. We have calculated the vesicle half-length along the field direction  $a_{max}/a = 1 + \sqrt{5/4\pi} f_{20}$  from Eq. 43 using the initial membrane tension  $\sigma_0$  as the only fitting parameter. The choice of  $\sigma_0$  as an adjustable variable is reasonable considering that the equilibrium membrane tension can not be controlled experimentally and it is not known a priori. The theoretical vesicle shapes are in a good agreement with the experimental data, albeit the onset of the decrease in the vesicle

deformation is overestimated. The fitted values for the initial tensions are of the same order of magnitude as in earlier work (20).

Some of the discrepancy between theory and experiment in the MHz frequency range could be ascribed to the omission of unsteady fluid motion, conductivity dispersion in the bulk electrolyte, or effects due to electric double layers.

We have used a quasi-steady approximation, tantamount to ignoring  $\rho\partial\mathbf{v}/\partial t$  in the equations of motion Eq. 14. Unsteady fluid motion is slower than a fully developed quasi-steady flow, resulting in weaker deforming stresses. Accordingly, vesicle deformation under unsteady flow conditions would be smaller. A quick estimate shows that temporal fluid acceleration becomes important at frequencies  $\omega \gg \eta/\rho a^2 \sim 10kHz$  (51).

The frequency at which vesicle deformation begins to decrease is also comparable to the inverse of the shortest of the interior and exterior fluid bulk charging times,  $t_c = \min\{t_{c,in}, t_{c,ex}\}$ . The charging time  $t_c$  is also interpreted as the time for the polarization of the screening cloud around an ion (43). If  $\omega > 2\pi/t_c$ , the ion atmosphere becomes distorted, which leads to increase in the conductivity (Debye-Falkenhagen effect). If  $t_c = t_{c,in}$ , the increase of inner fluid conductivity could possibly decrease the tendency for oblate deformations.

Another possible explanation for the fact that at high frequencies the observed vesicle deformation is smaller than the theoretically predicted one is that the theoretical membrane tension is underestimated. First, in the current model, the membrane tension increases solely due to flattening of the shape fluctuations by the electric forces. We have included only the contribution from the  $f_{20}$  mode in the apparent excess area. However, due to the area constraint (see Eq. 36) a decrease of  $f_{20}$  should be compensated by an increase in the amplitudes of the other shape modes. If all modes are accounted for, the apparent excess area would be larger and hence the tension would be higher (see Eq. 38). Second, electric double layers (EDLs) give rise to an additional increase of the membrane tension (26, 69). The electric field acting on the charges in the Debye layers on the interior and exterior sides of the membrane creates extensional stresses near the membrane that act to reduce membrane area, which is equivalent to increasing the tension (69). The calculation of the EDL contribution to the membrane tension is a complicated problem that has been solved only for a planar membrane (26, 69). Accounting for this effect in the case of a vesicle is a challenging task that we postpone to future study. At this time we assume that the EDL tension is constant. Figure 9 illustrates the frequency dependence of vesicle shape for  $\Lambda = 4.5$  and  $\Lambda = 0.4$  computed from Eq. 43 with  $\sigma_h$  as an adjustable parameter corresponding to the EDL tension. The somewhat surprising agreement between theory and experiment prompts further investigation.

Next, we focus on the prolate-oblate transition at lower frequencies, which previously eluded theoretical interpretation but is correctly captured by our theoretical model. Figure 10 shows the experimentally measured transition frequency  $\omega_1$  for 28 vesicles with different sizes and conductivity conditions. The theoretically predicted dependence of the transition frequency on the conductivity ratio agrees very well with the experimental data. Note that the scatter in the data is due to variations in vesicle sizes and conductivity conditions. Differences in the vesicle size affect the dimensionless membrane thickness  $x$ , and therefore we have plotted  $\omega_1(\Lambda)$  for three values of  $x$  corresponding to the average, the smallest, and the largest vesicle radii.

### 4.2.3 Oblate-prolate transition for $\Lambda < 1$ at high frequencies

At high frequencies  $\omega \gg \omega_1$ , the transmembrane potential vanishes, as seen in Figure 3. The electric tractions are given by the zero-thickness results Eq. 53 and Eq. 54 in Appendix C.1. The

forcing term  $C^{\text{el}}$  in the shape evolution Eq. 42 changes sign at a frequency

$$\Omega_2 = \left[ \frac{4S - (\Lambda + 1)^2}{(S - 1)^2} \right]^{\frac{1}{2}}. \quad (44)$$

Correspondingly, the vesicle deformation changes from oblate to prolate at this frequency. The transition frequency  $\Omega_2$  becomes very large when the dielectric constants of the fluids are comparable. For vesicles filled with sucrose and suspended in glucose solutions this frequency is about 1 GHz, which is in the frequency range where electric tractions have already become too small to deform the vesicle. Thus this oblate-prolate transitions was not observed in the experiments of Aranda et al. (1); instead, the vesicles become spherical. Thus far, the prolate-oblate transition has been reported only for drops (70).

If  $\Omega_2 < \omega_1$ , the oblate deformation would be impossible. This situation arises if the membrane becomes highly conducting, e.g., because of poration. Another possibility is a thick membrane or small vesicle with

$$\frac{h}{a} > \frac{(\Lambda + 2)^2 S_m}{(S + 2)(2\Lambda + G_m(\Lambda + 2))} \quad (45)$$

where  $S_m = \epsilon_{\text{mm}}/\epsilon_{\text{ex}}$ . For a typical bilayer thickness of  $5\text{nm}$  this condition holds for vesicle size below  $100\text{nm}$ . This prediction is in agreement with experimental studies of nano-sized vesicles (68) that have reported only prolate deformations.

The oblate-prolate transition is independent of membrane properties; it is analogous to the one observed with drops (70, 71). It is also independent of the viscosity ratio because the electrohydrodynamic flow stops at steady state due the interface immobilization by gradients in the membrane tension.

#### 4.2.4 The effective dipole theory does not predict the prolate-oblate transition

The effective dipole theory, summarized in Appendix C.2, models the cell as a sphere with effective permittivity. The theory successfully explains the dielectrophoresis and electrorotation of cells, because it correctly describes the perturbation due to the cell in the exterior electric field. However, the internal electric field is not physical, which leads to incorrect interior Maxwell stress and electric force distribution on the membrane. Accordingly, the predicted deformation is oblate at low frequencies (23), which is at odds with the experimental observations with vesicles (1).

Figure 11 compares the predictions of our model and the effective dipole theory for the electric tractions. It shows that the two models agree at frequencies  $\omega > \omega_1$ , where the transmembrane potential has vanished. At low frequencies, where the field inside the vesicle is zero, the effective dipole theory would correctly predict the electric tractions if only the contribution from the exterior electric field is taken into account. However, at intermediate frequencies, where the vesicle interior participates in the conduction process and the transmembrane potential is still significant, i.e.,  $\omega \sim \omega_1$ , the effective dipole theory diverges from our model as well as experimental observations (1).

## 5 Conclusions and outlook

We have developed a theory that explains the observed morphological transitions of vesicles in a uniform AC electric field, in particular, the shape dependence on the field frequency and conductivity ratio between the inner and outer fluids. Prolate deformations at low frequencies have purely dielectric origin and result from electric pressure due to polarization charges pulling the vesicle at the poles. Oblate deformations, however, result from induced free surface charges, which cause

negative pressure and transient electrohydrodynamic flow. The prolate-oblate transition at low frequencies depends on the membrane capacitance and conductance. At high frequencies, electric stresses become negligible and do not affect the vesicle equilibrium quasi-spherical shape. The theory also predicts a high-frequency oblate-prolate transition, which is analogous to the one observed with drops: it is independent of the membrane electric properties and depends only on the conductivities of inner and outer fluids. The transition frequency, however, is not given by the Maxwell-Wagner polarization time, but is determined by electrohydrodynamics.

We have considered the problem of vesicle electrodeformation from a mechanical point of view. In this new approach, vesicle shape is determined by balancing forces exerted on the interface, not by minimizing the bending and electrostatic energies as in earlier work. Thus, our formalism can be applied to study transient vesicle electrodeformation. Furthermore, it can be easily extended to electric fields of arbitrary symmetry as well as to situations in which both external electric and flow fields are present.

Our current theory is a first step in a systematic study of the electrohydrodynamics of deformable cells and, as such, some potentially important effects are neglected. First, our treatment assumes that all media are electrically homogeneous and is based on solutions of Laplace's equation. This approach requires that the Debye length of the media is small compared to the radius of the vesicle or the thickness of the membrane. Thus, our theory might break down at low conductivities and frequencies. Electric double layers may also increase the membrane tension (26). Second, the model does not include shear elasticity of the membrane, which is essential in the mechanics of the red blood cell (16). Third, the membrane is assumed to be non-permeable to ions. However, at low frequencies, the duration of the application of the electric field may be sufficient to porate the membrane (62). An electric current due to ion movement through field-induced pores would affect the electric field (28), and therefore vesicle shapes. Last, but not least, the conductivity of the electrolyte solutions may exhibit frequency dispersion. Electrokinetic effects, the role of shear elasticity, membrane poration, and membrane charge represent interesting and challenging problems. We hope that our work will stimulate future research on these topics.

## 6 Acknowledgments

PV thanks Thomas Powers and Margarita Staykova for stimulating discussions.

## A List of symbols

subscript  $r$  denotes *radial*  
subscript  $\theta$  denotes *tangential*  
sub/superscript “el” denotes *electric*  
sub/superscript “hd” denotes *hydrodynamic*  
sub/superscript “mm” denotes *membrane*  
sub/superscript “in” denotes *interior*  
sub/superscript “ex” denotes *exterior*  
superscript \* denotes *complex conjugate*  
 $Re[]$  denotes Real part of [ ]  
 $Im[]$  denotes Imaginary part of [ ]

$a$  vesicle radius

$C_m$  membrane capacitance

$Ca$  capillary number  
 $E$  electric field  
 $f_{jm}$  shape deformation parameter  
 $G_m$  membrane conductivity  
 $h$  membrane thickness  
 $H$  mean curvature  
 $p$  pressure  
 $S$  permittivity ratio  
 $t$  time  
 $\mathbf{T}$  bulk stress  
 $\mathbf{v}$  fluid velocity  
 $V_m$  transmembrane potential  
 $x = h/a$  dimensionless membrane thickness  
 $Y_{jm}$  spherical harmonic  
  
 $\eta$  viscosity  
 $\rho$  density  $\lambda$  conductivity  
 $\epsilon$  permittivity  
 $\Lambda$  conductivity ratio  
 $\chi$  viscosity ratio  
 $\omega_1$  frequency of the prolate-oblate transition  
 $\omega_2$  frequency corresponding to the inverse Maxwell-Wagner polarization time  
 $\Omega_2$  frequency of the oblate-prolate transition  
 $\Phi$  electric potential  
 $\tau$  tractions  
 $\sigma$  membrane tension  
 $\kappa$  bending rigidity  
 $\Delta$  excess area

## B Spherical harmonics

The normalized spherical scalar harmonics are defined as (72)

$$Y_{jm}(\theta, \varphi) = \left[ \frac{2j+1}{4\pi} \frac{(j-m)!}{(j+m)!} \right]^{\frac{1}{2}} (-1)^m P_j^m(\cos \theta) e^{im\varphi}, \quad (46)$$

where  $(r, \theta, \varphi)$  are the spherical coordinates, and  $P_j^m(\cos \theta)$  are the Legendre polynomials. For example

$$Y_{10} = \frac{3}{\sqrt{4\pi}} \cos \theta. \quad (47)$$

## C Electrostatic field and stresses for a spherical shell

### C.1 Our model: A sphere with interfacial capacitance and conductivity

Schwann et al. (44, 64) have solved the problem for the electric field about a spherical shell with radius  $a$  and shell thickness  $h$  to obtain Eq. 8 for the potential difference between the inner and outer shell surfaces. Assuming a very thin shell  $h/a \ll 1$ , we can approximate the membrane

with a two-dimensional interface that possesses capacitance. Accordingly, the spherical shell is approximated by a sphere with a discontinuous potential at the interface.

Solving Eq. 7 with the boundary conditions Eq. 8, Eq. 9 and Eq. 10 leads to

$$\begin{aligned}\Phi^{\text{ex}} &= -[r + P^{\text{ex}}r^{-2}] \exp(i\omega t) \cos \theta, \\ \Phi^{\text{in}} &= -P^{\text{in}}r \exp(i\omega t) \cos \theta.\end{aligned}\tag{48}$$

where

$$\begin{aligned}P^{\text{ex}} &= d^\infty \frac{(-k_{\text{in}} + k_{\text{ex}}) + k_{\text{in}}V_m}{k_{\text{in}} + 2k_{\text{ex}}}, \\ P^{\text{in}} &= d^\infty k_{\text{ex}} \frac{3 - 2V_m}{k_{\text{in}} + 2k_{\text{ex}}},\end{aligned}\tag{49}$$

and  $k$  denote the dimensionless complex conductivities of the inner and outer fluids

$$k_{\text{in}} = \Lambda + i\omega S, \quad k_{\text{ex}} = 1 + i\omega.\tag{50}$$

The tractions are computed from the Maxwell stress tensor. The radial (pressure) component is given by

$$\tau_r^{\text{el}} = \frac{1}{32\pi} [-2(\tau_1^2 + \tau_2^2)S + 5\tau_3^2 - 2d^\infty\tau_3 + 5\tau_4^2 + 2(d^\infty)^2],\tag{51}$$

and the tangential (shearing) component is

$$\tau_\theta^{\text{el}} = -\frac{3}{8\pi} [(\tau_1^2 + \tau_2^2)S + 2\tau_3^2 + (d^\infty)\tau_3 + 2\tau_4^2 - (d^\infty)^2],\tag{52}$$

where  $\tau_1 = \text{Re}[P^{\text{in}}]$ ,  $\tau_2 = \text{Im}[P^{\text{in}}]$ ,  $\tau_3 = \text{Re}[P^{\text{ex}}]$ ,  $\tau_4 = \text{Im}[P^{\text{ex}}]$ .  $\text{Re}[\ ]$  and  $\text{Im}[\ ]$  denote real and imaginary part. Taking the zero-thickness limit,  $x = 0$ , our solution reduces to the result for a spherical drop (70)

$$\tau_r^{\text{el},\text{drop}} = \frac{3}{8} (1 + \Lambda^2 - 2S + (S - 1)^2 S \omega^2) (2 + S)^2 (\omega^2 + \omega_2^2)^{-1},\tag{53}$$

$$\tau_\theta^{\text{el},\text{drop}} = \frac{9}{2} (\Lambda - S) (2 + S)^2 (\omega^2 + \omega_2^2)^{-1},\tag{54}$$

where  $\omega_2$  is given by Eq. 35

The effective charge density is calculated from Eq. 9

$$Q(\omega, t) = q_c(\omega) \cos(\omega t) + q_s(\omega) \sin(\omega t),\tag{55}$$

where

$$q_s(\omega) = 2\tau_4 + S\tau_2, \quad q_c(\omega) = d^\infty - 2\tau_3 - S\tau_1\tag{56}$$

The frequency dependence of the charge density can be cast into the form

$$Q(\omega, t) = \bar{Q}(\omega) \cos(\omega t + \psi),\tag{57}$$

where the amplitude is  $\bar{Q}(\omega) = [q_s + q_c]^{\frac{1}{2}}$ , and the phase shift is  $\psi = q_s/q_c$ .

## C.2 The effective sphere model

The dipole theory models the cell as a sphere with an effective permittivity (13, 14)

$$k_{\text{in}}^{\text{eff}} = k_{\text{in}} \left[ (1-x)^{-3} + 2 \frac{k_{\text{in}} - k_{\text{mm}}}{k_{\text{in}} + 2k_{\text{mm}}} \right] \left[ (1-x)^{-3} - \frac{k_{\text{in}} - k_{\text{mm}}}{k_{\text{in}} + 2k_{\text{mm}}} \right]^{-1}, \quad (58)$$

where

$$k_{\text{in}} = \Lambda + i\omega S, \quad k_{\text{mm}} = \Lambda_{\text{mm}} + i\omega S_{\text{mm}}. \quad (59)$$

The electric field is described by an electric potential

$$\Phi^{\text{ex}} = -d^\infty \left[ r + r^{-2} \frac{(-k_{\text{in}}^{\text{eff}} + k_{\text{ex}})}{k_{\text{in}}^{\text{eff}} + 2k_{\text{ex}}} \right] \cos \theta, \quad \Phi^{\text{in}} = -rd^\infty k_{\text{ex}} \frac{3}{k_{\text{in}}^{\text{eff}} + 2k_{\text{ex}}} \cos \theta, \quad (60)$$

where a continuity of the potential across the interface is assumed.

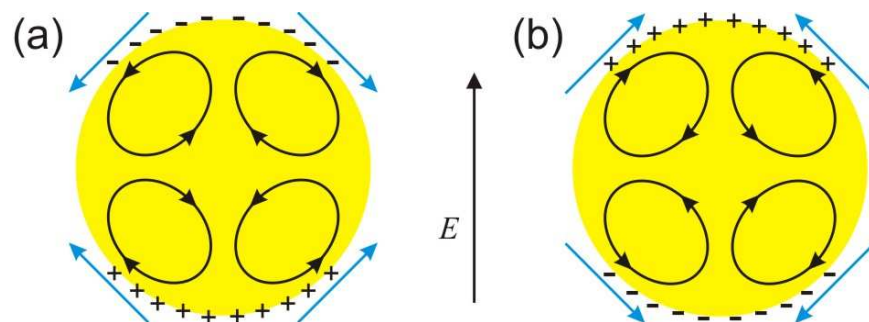


Figure 1: An illustration of the surface charge distribution and the streamlines of the electrohydrodynamic flow inside a drop (38, 70) or a vesicle. The corresponding direction of the tangential electric traction is denoted by arrows. (a) interior fluid less conducting than the exterior one,  $\Lambda/S < 1$ . The resulting shape is oblate because the EHD flow pushes fluid towards the equator; (b) interior fluid more conducting than the exterior one,  $\Lambda/S > 1$

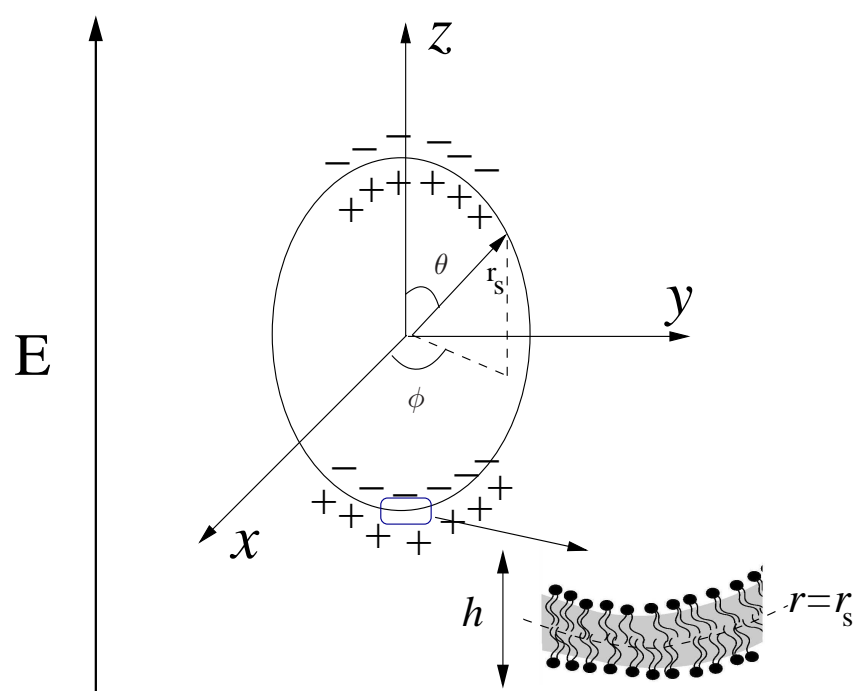


Figure 2: A sketch of a vesicle in a uniform electric field. The zoomed region of the interface illustrates the lipid bilayer structure of the membrane.

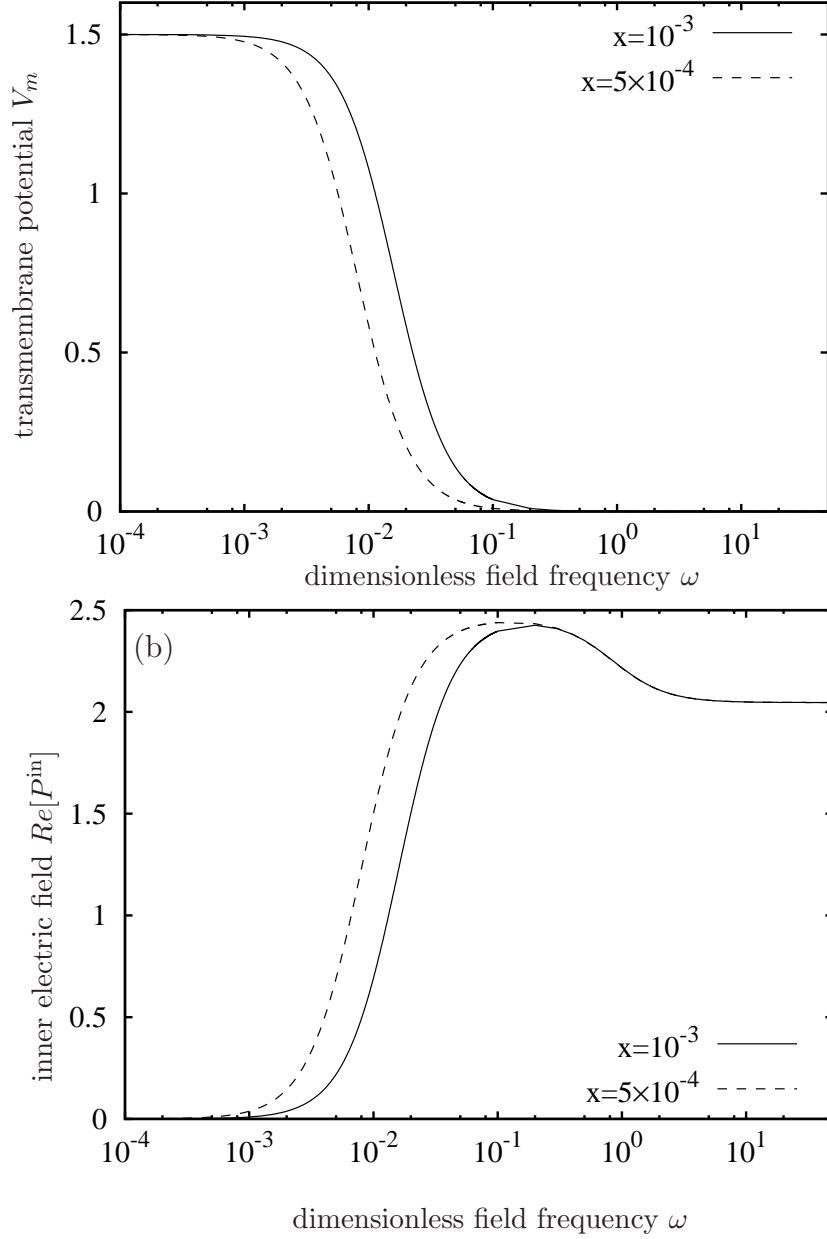


Figure 3: (a) Transmembrane potential at the poles  $\theta = 0, \pi$  calculated from Eq. 30, and (b) interior electric field calculated from Eq. 49 for a spherical shell with different membrane thickness,  $x = 5 \times 10^{-4}$  and  $x = 10^{-3}$ , in a uniform AC electric field.  $\Lambda = 0.5$ ,  $S = 1.001$ ,  $C_m = 0.025/x$ ,  $G_m = 0$ .

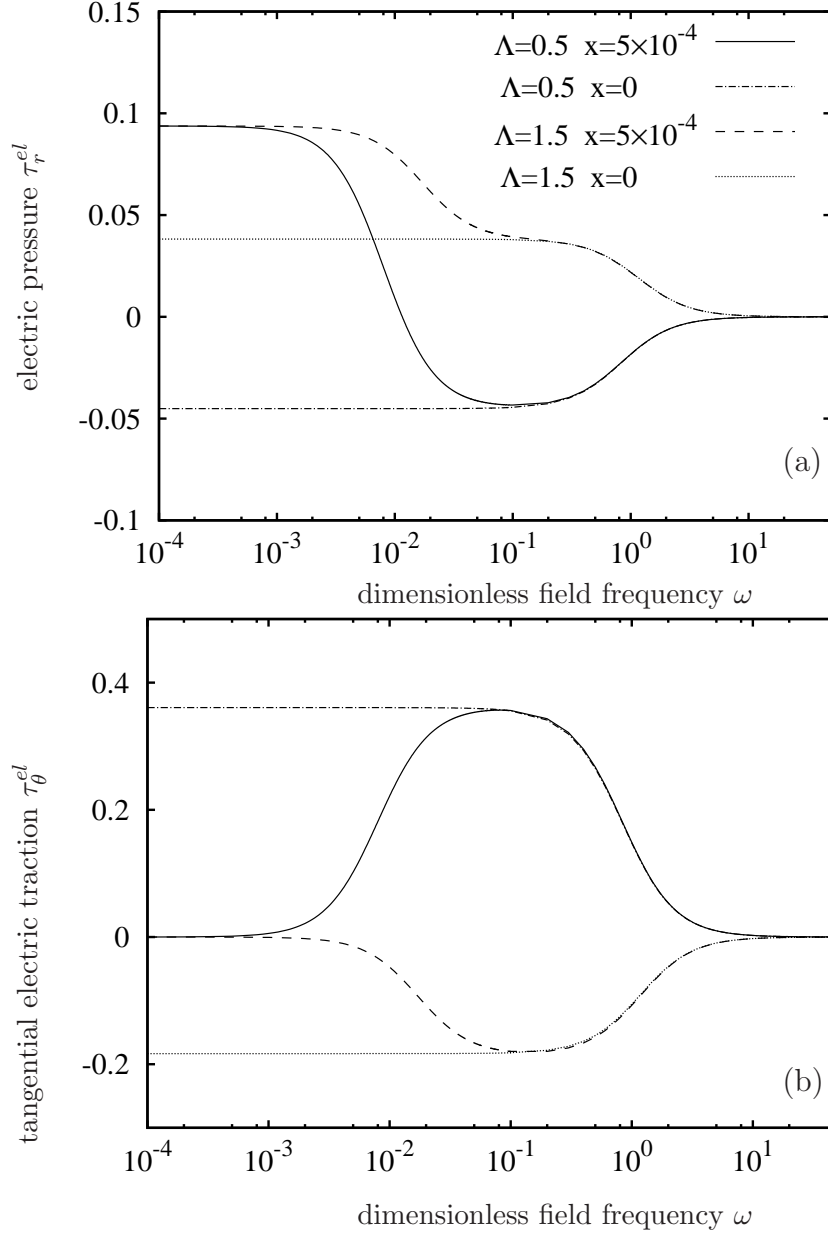


Figure 4: Electric tractions on the membrane as a function of the frequency for two conductivity ratios,  $\Lambda = 0.5$  and  $\Lambda = 1.5$ . (a) electric pressure calculated from Eq. 51; (b) tangential electric force calculated from Eq. 52. The values of the other physical parameters are  $S = 1.001$ ,  $C_m = 0.025/x$ ,  $G_m = 0$ . The electric tractions in the case of a droplet (the zero-membrane-thickness limit  $x = 0$ ) are also shown for comparison.

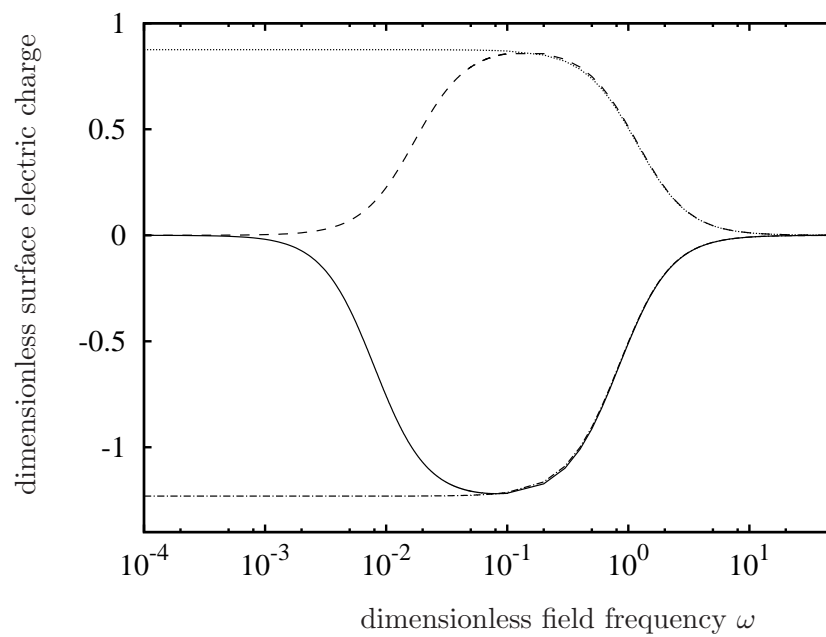


Figure 5: The absolute value of the amplitude of the interfacial charge density at the poles  $\theta = 0, \pi$ . Notation and parameter values are the same as in Fig. 4

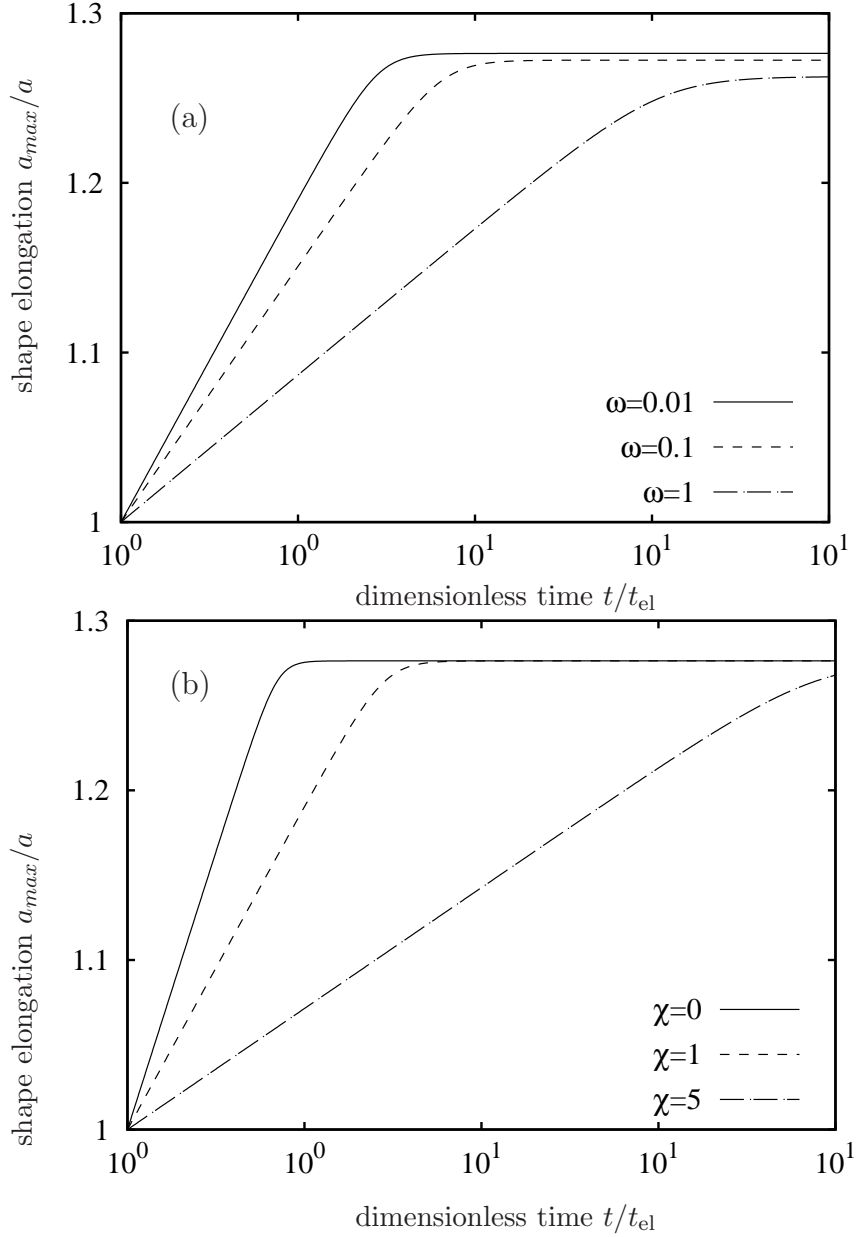


Figure 6: Evolution of the ellipsoidal deformation  $a_{max}/a$ , calculated from Eq. 42, of a quasi-spherical vesicle upon application of a uniform AC electric field. (a) for frequencies  $\omega = 0.01, 0.1, 1$  and the same viscosity ratio  $\chi = 1$ . (b) for viscosity ratios  $\chi = 0, 1, 5$  and the same the AC field frequency is  $\omega = 0.01$ . The values of the physical parameters are  $\Lambda = 1.5$ ,  $x = 5 \times 10^{-4}$ ,  $S = 1.001$ ,  $G_m = 0$ , and  $C_m = 50$ .  $Ca = 6837$  corresponds to  $E_0 = 2 \times 10^4 V/m$ ,  $\eta_{ex} = 10^{-3} Pa.s$ ,  $\kappa = 10 k_B T$  and  $a = 10 \mu m$ .

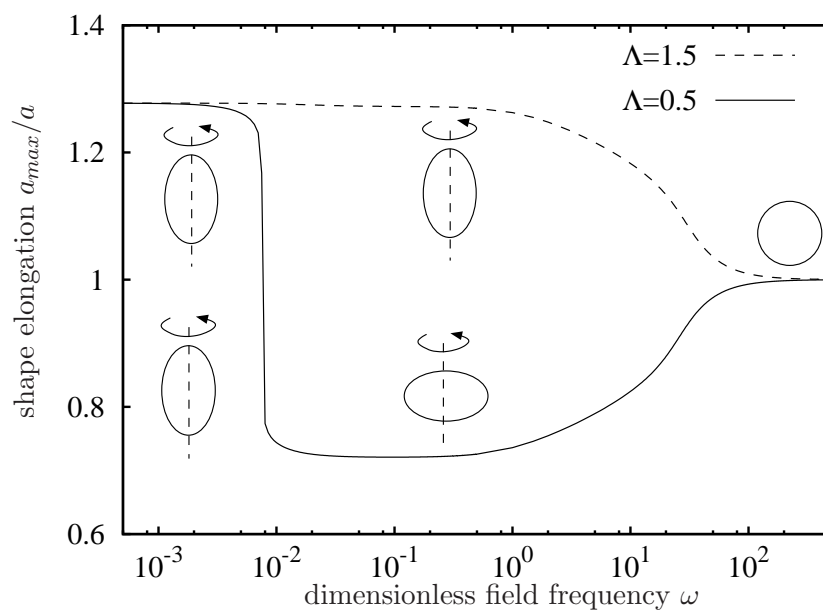


Figure 7: Ellipsoidal deformation  $a_{max}/a$  of vesicles in uniform AC electric field as a function of the dimensionless frequency for two conductivity ratios  $\Lambda = 0.5$  and  $\Lambda = 1.5$ . Other parameters are the same as in Figure 6

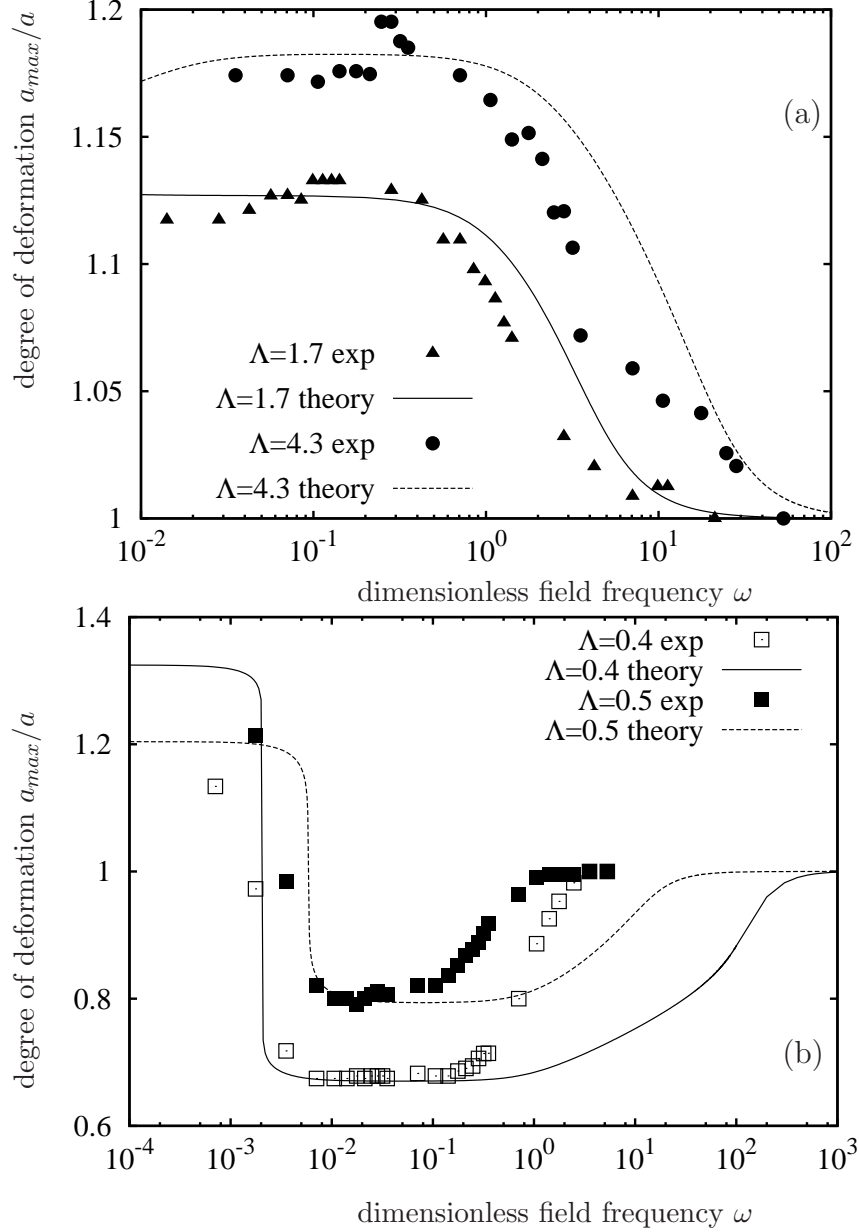


Figure 8: Comparison between theory and the experimental data of Aranda et al. (1) for (a). prolate deformations. The fitted initial tensions are  $\sigma_0 = 20000$  (corresponding to  $1.1 \times 10^{-3} mN/m$ ) for  $\Lambda = 1.7$  and  $\sigma_0 = 3000$  ( $1.6 \times 10^{-4} mN/m$ ) for  $\Lambda = 4.3$ . (b). oblate deformations. The fitted initial tensions are  $\sigma_0 = 1$  ( $5.6 \times 10^{-8} mN/m$ ) for  $\Lambda = 0.4$  and  $\sigma_0 = 100$  ( $2.5 \times 10^{-5} mN/m$ ) for  $\Lambda = 0.5$ .

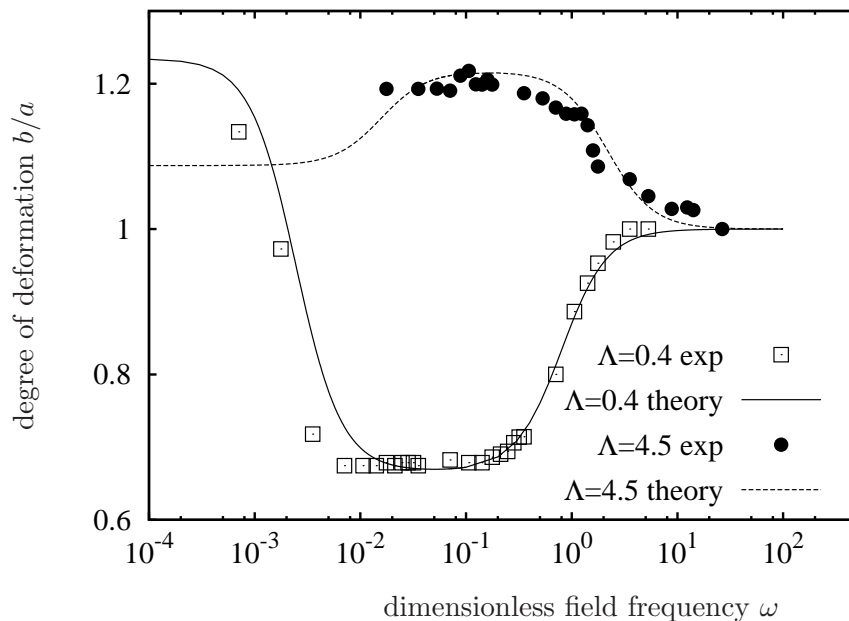


Figure 9: Comparison between theory (line) and the experimental data (symbols) of Aranda et al. (1) assuming constant tension. The theoretical line is calculated from Eq. 43 for  $\Lambda = 4.5$  with  $\sigma_h = 40000$  (corresponding to  $5.3 \times 10^{-3} mN/m$ ), and for  $\Lambda = 0.4$  with  $\sigma_h = 55000$  ( $\sigma_h = 3 \times 10^{-3} mN/m$ ).

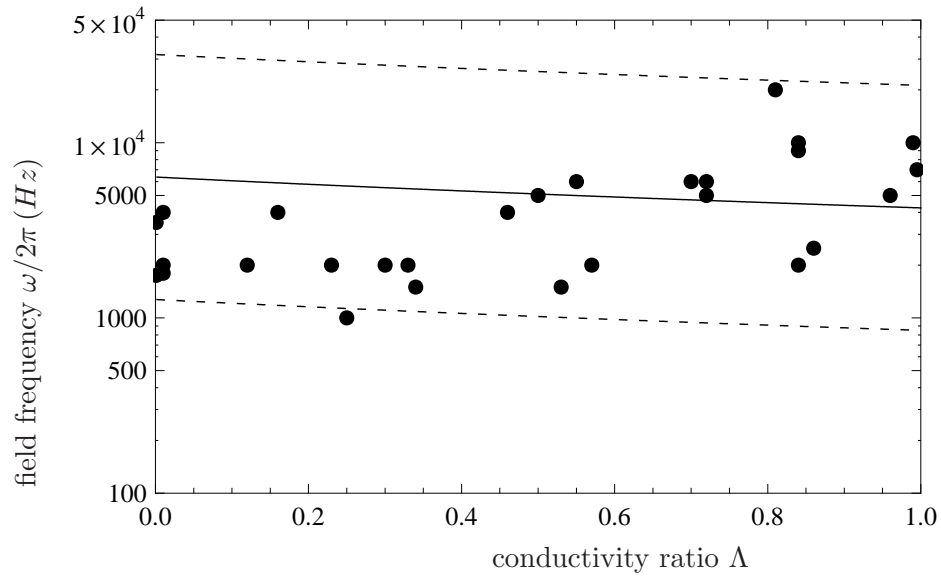


Figure 10: Prolate-oblate transition frequency for different conductivity ratios  $\Lambda$ . The points are experimental data (1, 32) for 28 vesicles with different size; the fluids conductivities are about  $10^{-4} S/m$ . The solid line is the theoretical prediction using  $x = 10^{-4}$  corresponding to vesicle radius  $a = 50 \mu m$ . The bottom dashed line is calculated using  $x = 2 \times 10^{-5}$  and the top dashed line is calculated using  $x = 5 \times 10^{-4}$ . The basic charging time is estimated to be  $t_c = 10^{-7} s$ .

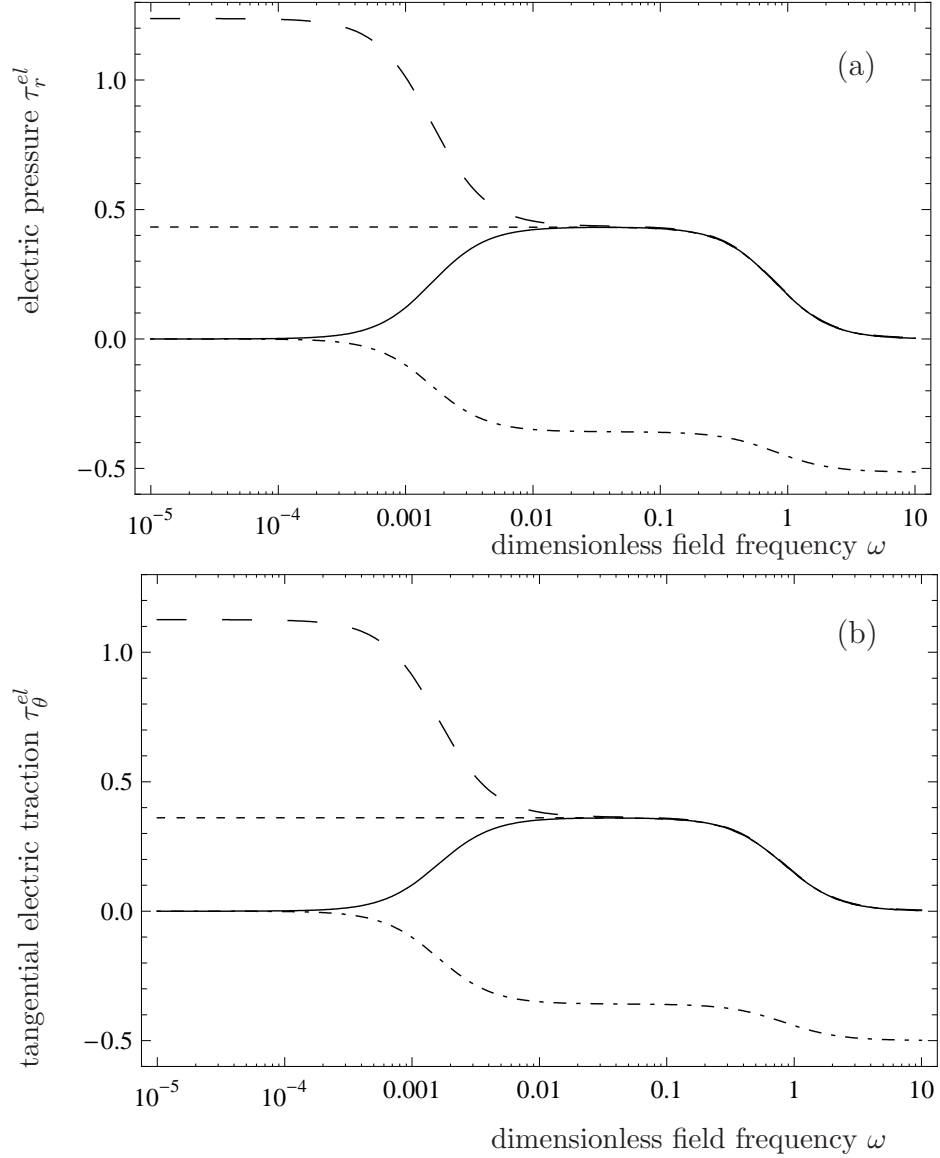


Figure 11: The electric tractions according to our model (solid line), the drop model (short-dashed line), the effective dipole theory (long-dashed line) and only exterior field contribution in the effective dipole theory (dot-dashed line). (a) electric pressure (b) tangential tractions. Parameters are:  $\Delta = 0.5$ ,  $\Lambda = 1.5$ ,  $x = 5 \times 10^{-4}$ ,  $G_m = 0$ ,  $C_m = 50$  and  $Ca = 684$ .

## References

1. Aranda, S., K. A. Riske, R. Lipowsky, and R. Dimova, 2008. Morphological transitions of vesicles induced by AC electric fields. *Biophys. J.* 95:L19–L21.
2. Zhao, M., B. Song, J. Pu, T. Wada, B. Reid, G. P. Tai, F. Wang, A. H. Guo, P. Walczysko, Y. Gu, T. Sasaki, A. Suzuki, J. V. Forrester, H. R. Bourne, P. N. Devreotes, C. D. McCaig, and J. M. Penninger, 2006. Electrical signals control wound healing through phosphatidylinositol-3-OH kinase- and PTEN. *Nature* 442:457–460.
3. Funk, R. H. W., and T. K. Monsees, 2006. Effects of Electromagnetic Fields on Cells: Physiological and Therapeutical Approaches and Molecular Mechanisms of Interaction. *Cells Tissues Organs* 182:59–78.
4. Voldman, J., 2006. Electrical Forces For Microscale Cell Manipulation. *Annu. Rev. Biomed. Eng.* 8:425–454.
5. Zimmermann, U., and G. A. Neil, 1996. Electromanipulation of cells. CRC Press, Boca Raton.
6. Neumann, E., A. E. Sowers, and C. A. Jordan, 1989. Electroporation and electrofusion in cell biology. Plenum Press, New York.
7. Chizmadzhev, Y. A., P. Kuzmin, and V. P. Pastushenko, 1985. Theory of the dielectrophoresis of vesicles and cells. *Biol. Mem.* 2:1147–1161.
8. Chizmadzhev, Y. A., P. Kuzmin, and V. P. Pastushenko, 1988. Dielectrophoresis and electrorotation of cells: unified theory for spherically symmetric cells with arbitrary structure of membrane. *Biol. Mem.* 5:65–78.
9. Turcu, I., and C. M. Lucaciu, 1989. Dielectrophoresis -a spherical shell model. *J. Phys. A* 22:985–993.
10. Jones, T. B., 1995. Electromechanics of particles. Cambridge University Press, New York.
11. Gimsa, J., and D. Wachner, 1999. A polarization model overcoming the geometric restrictions of the laplace solution for spheroidal cells: Obtaining new equations for field-induced forces and transmembrane potential. *Biophys. J.* 77:1316–1326.
12. Dolinsky, Y., and T. Elperin, 2006. Dynamics of a spheroidal particle in a leaky dielectric medium in an ac electric field. *Phys. Rev. E* 73:066607.
13. Foster, K. R., F. A. Sauer, and H. P. Schwan, 1992. Electrorotation and levitation of cells and colloidal particles. *Biophys. J.* 63:180–190.
14. Jones, T. B., 2003. Basic theory of dielectrophoresis and electrorotation. *IEEE Eng Med Biol Mag.* 22:33–42.
15. Miller, R. D., and T. B. Jones, 1993. Electro-orientation of ellipsoidal erythrocytes. Theory and experiment. *Biophys. J.* 64:1588–1595.
16. Engelhardt, H., and E. Sackmann, 1988. On the measurement of shear elastic moduli and viscosities of erythrocyte plasma membranes by transient deformation in high frequency electric fields. *Biophys. J.* 54:495–508.

17. Bryant, G., and J. Wolfe, 1987. Electromechanical stresses produced in the plasma membranes of suspended cells by applied electric fields. *J. Membr. Biol.* 96:129–139.
18. Poznanski, J., P. Pawlowski, and M. Fikus, 1992. Bioelectrorheological model of the cell. 3. Viscoelastic shear deformation of the membrane. *Biophys. J.* 61:612–620.
19. Helfrich, W., 1974. Deformation of lipid bilayer spheres by electric fields. *Z. Naturforsch.* 29c:182–183.
20. Kummrow, M., and W. Helfrich, 1991. Deformation of giant lipid vesicles by electric fields. *Phys. Rev. A* 44:8356–8360.
21. Winterhalter, M., and W. Helfrich, 1988. Deformation of spherical vesicles by electric fields. *J. Coll. Int. Sci.* 122:583–586.
22. Teissie, J., and T. Y. Tsong, 1981. Electric field induced transient pores in phospholipid bilayer vesicles. *Biochemistry* 20:1548–1554.
23. Sukhorukov, V., H. Mussauer, and U. Zimmermann, 1998. The effect of electrical deformation forces on the electropermeabilization of erythrocyte membranes in low- and high-conductivity media. *J. Membr. Biol.* 163:235–245.
24. Isambert, H., 1998. Understanding the electroporation of cells and artificial bilayer membranes. *Phys. Rev. Lett.* 80:3404–3407.
25. Sens, P., and H. Isambert, 2002. Undulation instability of lipid membranes under an electric field. *Phys. Rev. Lett.* 88:Art. No. 128102.
26. Lacoste, D., M. Lagomarsino, and J. Joanny, 2007. Fluctuations of a driven membrane in an electrolyte. *Europhys. Lett.* 77:18006.
27. Ambjornsson, T., M. A. Lomholt, and P. L. Hansen, 2007. Applying a potential across a biomembrane: Electrostatic contribution to the bending rigidity and membrane instability. *Phys. Rev. E* 75:051916.
28. Krassowska, W., and P. Filev, 2007. Modeling electroporation in a single cell. *Biophys. J.* 92:404–417.
29. Riske, K. A., and R. Dimova, 2005. Electro-deformation and poration of giant vesicles viewed with high temporal resolution. *Biophys. J.* 88:1143–1155.
30. Riske, K. A., and R. Dimova, 2006. Electric pulses induce cylindrical deformations on giant vesicles in salt solutions. *Biophys. J.* 91:1778–1786.
31. Dimova, R., S. Aranda, N. Bezlyepkina, V. Nikolov, K. A. Riske, and R. Lipowsky, 2006. A practical guide to giant vesicles. Probing the membrane nanoregime via optical microscopy. *J. Phys. Cond. Matt.* 18:S1151–S1176.
32. Dimova, R., K. A. Riske, S. Aranda, N. Bezlyepkina, R. L. Knorr, and R. Lipowsky, 2007. Giant vesicles in electric fields. *Soft matter* 3:817–827.
33. Peterlin, P., S. Svetina, and B. Zeks, 2007. The prolate-to-oblate shape transition of phospholipid vesicles in response to frequency variation of an AC electric field can be explained by the dielectric anisotropy of a phospholipid bilayer. *J. Phys. Cond. Phys.* 19:136220.

34. Hyuga, H., K. Kinoshita Jr., and N. Wakabayashi, 1991. Deformation of vesicles under the influence of strong electric fields. *Jpn. J. Appl. Phys.* 30:1141–1148.
35. Sauer, F. A., 1985. Interaction forces between microscopic particles in an external electromagnetic field. In A. Chiabrera, C. Nicolini, and H. P. Schwan, editors, Interactions between electromagnetic fields and cells, Plenum Press, 181–202.
36. Saville, D. A., 1997. Electrohydrodynamics: The Taylor-Melcher leaky dielectric model. *Annu. Rev. Fluid Mech.* 29:27–64.
37. Squires, T. M., and M. Z. Bazant, 2004. Induced-charge electro-osmosis and electrophoresis. *J. Fluid Mech.* 509:217–252.
38. Taylor, G. I., 1966. Studies in electrohydrodynamics. I. Circulation produced in a drop by an electric field. *Proc. Royal Soc. A* 291:159–166.
39. Melcher, J. R., and G. I. Taylor, 1969. Electrohydrodynamics - a review of role of interfacial shear stress. *Annu. Rev. Fluid Mech.* 1:111–146.
40. Staykova, M., R. Lipowsky, and R. Dimova, 2008. Membrane flow patterns in multicomponent giant vesicles induced by alternating electric fields. *Soft Matter* 4:2168–2171.
41. Seifert, U., 1995. The concept of effective tension for fluctuating vesicles. *Z. Phys. B* 97:299–309.
42. Evans, E., and W. Rawicz, 1990. Entropy driven tension and bending elasticity in condensed-fluid membranes. *Phys. Rev. Lett.* 64:2094–2097.
43. Bazant, M. Z., K. Thornton, and A. Ajdari, 2004. Diffuse-charge dynamics in electrochemical systems. *Phys. Rev. E* 70:021506.
44. Schwan, H. P., 1989. Dielectrophoresis and rotation of cells. In E. Neumann, A. E. Sowers, and C. A. Jordan, editors, Electroporation and electrofusion in cell biology, Plenum Press, 3–21.
45. Kinoshita Jr., K., I. Ashikawa, N. Saita, H. Yoshimura, H. Itoh, K. Nagayama, and A. Ikegami, 1988. Electroporation of cell membrane visualized under a pulsed laser fluorescence microscope. *Biophys. J.* 53:1015–1019.
46. Seifert, U., 1999. Fluid membranes in hydrodynamic flow fields: Formalism and an application to fluctuating quasispherical vesicles. *Eur. Phys. J. B* 8:405–415.
47. Mitov, M. D., P. Meleard, M. Winterhalter, M. I. Angelova, and P. Bothorel, 1993. Electric-field-dependent thermal fluctuations of giant vesicles. *Phys. Rev. E* 48:628–631.
48. Needham, D., and R. M. Hochmuth, 1989. Electromechanical permeabilization of lipid vesicles. Role of membrane tension and compressibility. *Biophys. J.* 55:1001–1009.
49. Nelson, P., 2004. Life in the Slow Lane: The Low Reynolds-Number World. In Biological Physics: Energy, Information, Life, Freeman, 158–194.
50. Leal, L. G., 1980. Particle motions in a viscous fluid. *Ann. Rev. Fluid Mech* 12:435–476.
51. Sozou, C., 1972. Electrohydrodynamics of a liquid drop - time-dependent problem. *Proc. Royal Soc. A* 331:263–272.

52. Leal, L. G., 1992. *Laminar Flow and Convective Transport Processes*. Butterworth-Heinemann, Boston.
53. Petrov, A. G., 2006. Electricity and mechanics of biomembrane systems: Flexoelectricity in living membranes. *Analytica Chimica Acta* 568:70–83.
54. Raphael, R. M., A. S. Popel, and W. E. Brownell, 2000. A Membrane Bending Model of Outer Hair Cell Electromotility. *Biophys. J.* 78:2844–2862.
55. Seifert, U., 1997. Configurations of fluid membranes and vesicles. *Advances in physics* 46:13–137.
56. Evans, E., and A. Yeung, 1994. Hidden dynamics in rapid changes of bilayer shape. *Chem. Phys. Lipids* 73:39–56.
57. Seifert, U., and S. A. Langer, 1993. Viscous modes of fluid bilayer membranes. *Europhys. Lett.* 23:71–76.
58. Pott, T., and P. Meleard, 2002. The dynamics of vesicle thermal fluctuations is controlled by intermonolayer friction. *Europhys. Lett.* 59:87–93.
59. Miao, L., M. A. Lomholt, and J. Kleis, 2002. Dynamics of shape fluctuations of quasi-spherical vesicles revisited. *Eur. Phys. J. E.* 9:143–160.
60. Zimmermann, U., 1982. Electric field mediated fusion and related electrical phenomena. *Biochim. Biophys. Acta* 694:227–277.
61. Teissie, J., M. Golzio, and M. P. Rols, 2005. Mechanisms of cell membrane electropermeabilization: A minireview of our present (lack of ?) knowledge. *BBA* 1724:270–280.
62. Harbich, W., and W. Helfrich, 1979. Alignment and opening of giant lecithin vesicles by electric field. *Z. Naturforsch. A* 34:1063–1065.
63. Chang, D. C., 1989. Cell poration and cell fusion using an oscillating electric field. *Biophys. J.* 56:641–652.
64. Grosse, C., and H. P. Schwan, 1992. Cellular membrane potentials induced by alternating fields. *Biophys. J.* 63:1632–1642.
65. Vlahovska, P. M., and R. Gracia, 2007. Dynamics of a viscous vesicle in linear flows. *Phys. Rev. E* 75:016313.
66. Danker, G., T. Biben, T. Podgorski, C. Verdier, and C. Misbah, 2007. Dynamics and rheology of a dilute suspension of vesicles: higher order theory. *Phys. Rev. E* 76:041905.
67. Lebedev, V. V., K. S. Turitsyn, and S. S. Vergeles, 2008. Nearly spherical vesicles in an external flow. *New J. Phys.* 10:043044.
68. Kakorin, S., T. Liese, and E. Neumann, 2003. Membrane curvature and high-field electroporation of lipid bilayer vesicles. *J. Phys. Chem. B* 107:10243–10251.
69. Lacoste, D., G. I. Menon, M. Z. Bazant, and J. F. Joanny, 2009. Electrostatic and electrokinetic contributions to the elastic moduli of a driven membrane. *Eur. Phys. J. E* DOI: 10.1140/epje/i2008-10433-1.

70. Torza, S., R. Cox, and S. Mason, 1971. Electrohydrodynamic deformation and burst of liquid drops. *Phil. Trans. Royal Soc. A* 269:295–319.
71. Vizika, O., and D. A. Saville, 1992. The electrohydrodynamic deformation of drops suspended in liquids in steady and oscillatory electric fields. *J. Fluid Mech.* 239:1–21.
72. Varshalovich, D. A., A. N. Moskalev, and V. K. Kheronskii, 1988. Quantum Theory of Angular Momentum. World Scientific, Singapore.